

Diffusion-Weighted Whole-Body MRI at 3 Tesla for the Detection and Discrimination of Pulmonary Tumors

Petra Murtz^{1*}, Marius G. Kaschner¹, Brigitte Hinterthaler¹, Birgit Simon¹, Hojjat Ahmadzadehfar², Dirk Skowasch³, Hans H. Schild¹, Winfried A. Willinek¹, Guido M. Kukuk¹

¹Department of Radiology, University of Bonn, Germany

²Department of Nuclear Medicine, University of Bonn, Germany

³Department of Medicine, University of Bonn, Germany

*Corresponding author: Petra Murtz, Radiologische Klinik der Universität Bonn, Sigmund-Freud-Straße 25, 53105 Bonn, Germany, Tel: +49 228 287 14496/ Fax: +49 228 287 9014496; E-mail: petra.muertz@ukb.uni-bonn.de

Abstract

Objective: To evaluate diffusion-weighted whole-body MRI with background body signal suppression (DWIBS) at 3.0 T for pulmonary lesion detection and characterization.

Materials and Methods: 19 patients with 25 pulmonary lesions were examined with DWIBS using 2 b-values ($b = 0$ and 1000 s/mm^2) and partly additionally with DWIBS using 3 b-values ($b = 0, 50, 1000 \text{ s/mm}^2$). DWIBS was compared to FDG PET. For characterization of hyperintense lesions by DWIBS, Lesion-to-Spinal cord Ratio (LSR) and apparent diffusion coefficient ADC were analyzed. From repeated measurements, the Coefficient of Variation (CV) was calculated. From 3-b-value data, the ADC(0,1000) and ADC(50,1000) values were compared in order to assess perfusion influences.

Results: Sensitivity and specificity of detecting malignant lesions were comparable for DWIBS and FDG PET. Malignant compared to benign lesions had lower ADC(0,1000) and higher LSR values. CV of LSR was more than a factor of 8 higher than CV of ADC(0,1000) (23.9% vs 2.9%, $P = 0.012$). Perfusion effects were largest for metastases, medium for adenocarcinoma and benign lesions, and lowest for squamous cell carcinoma.

Conclusion: DWIBS at 3.0 T is appropriate for lesion detection and characterization. ADC analysis is superior to signal intensity ratio determination with respect to repeatability. An analysis of perfusion influences provides additional information.

Keywords: DW MRI; DWIBS; 3.0 T; FDG PET/CT; Lung Cancer; Pulmonary Lesions

Received Date: March 16, 2017

Accepted Date: April 12, 2017

Published Date: April 19, 2017

Citation: Murtz, P., et al. Diffusion-Weighted Whole-Body MRI at 3 Tesla for the Detection and Discrimination of Pulmonary Tumors. (2017) *Bioinfo Proteom Img Anal* 3(2): 214-221.

DOI: 10.15436/2381-0793.17.1431



Introduction

Standard imaging techniques provide a high sensitivity for detection of pulmonary lesions however specificity is limited^[1]. Diagnostic accuracy can be improved by using functional techniques such as Dynamic Contrast Enhanced (DCE) CT, ¹⁸F-labeled 2-Fluoro-2-Deoxy-D-Glucose (FDG) Positron Emission Tomography (PET), ^{99m}Tc-depreotide Single Photon Emission Computed Tomography (SPECT), DCE MRI, and Diffusion-Weighted Imaging (DWI)^[2].

DWI is a noninvasive, radiation- and contrast agent-free MRI method, which detects the microscopic motion of water molecules within a voxel, providing information on the biophysical properties of tissue, such as cell organization, cell density, microstructure, and microcirculation^[3]. With recent ad-

vancements, technological challenges of chest DWI have at least partially been solved^[3,4]. In comparison to DCE CT, DCE MRI, FDG PET and SPECT, with DWI lower sensitivity but higher specificity for differentiation of malignant from benign lung lesions was found^[2,5]. Recent studies even found higher sensitivity and equal specificity for DWI compared to FDG PET^[6,7]. The detection rate of DWI for tumor recurrence and metastasis is similar to PET/CT^[8]. As an adjunct to DCE MRI, DWI can improve the diagnostic accuracy of DCE MRI^[9].

A general problem of chest DWI is that image quality is limited by susceptibility-induced artefacts at air-tissue and bone-soft tissue interfaces and by motion artefacts due to breathing, heartbeat and vascular pulsation^[3]. Most studies were performed at 1.5 T^[3,5,7,8,10,11]. In conventional DWI spectral selective fat suppression methods were used, which are sensitive



to magnetic field inhomogeneity. For the chest, a more robust DWI technique is provided by diffusion-weighted whole body imaging with background body signal suppression (DWIBS)^[3] as introduced by Takahara et al^[12]. DWIBS is acquired during free breathing and using Short TI Inversion Recovery (STIR) fat suppression. Although offering less Signal-to-Noise Ratios (SNR) in comparison to conventional DWI, DWIBS has proven to be less prone to magnetic field inhomogeneity and therefore more suitable for imaging of the lungs.

Higher field strengths offer increased SNR. However, technological challenges with respect to artefacts, radio frequency inhomogeneity, and fat suppression, are even higher at 3.0 T compared to 1.5 T^[13,14]. Up to now, only little experience exists for chest DWI at 3.0 T^[3,15-18], especially for the DWIBS variant^[9,13,14,19]. However, there is growing interest, especially due to the increased clinical use of combined FDG-PET/MRI scanners working at 3.0 T^[20].

Therefore, the aim of this study was to evaluate DWIBS at 3.0 T for pulmonary lesion detection and characterization.

Materials and methods

Patient Population

The study was approved by the local institutional review board, and written informed consent was obtained from all patients. 19 consecutive patients (12 male, 7 female; mean age: 65 years; age range: 27 - 79 years) with 25 pulmonary lesions suspected of being primary lung cancers at chest CT were included. In order to avoid partial volume effects, only lesions with a size larger than 10 mm were included. The final diagnosis was lung cancer in 14 lesions (8 adenocarcinomas, 4 squamous cell carcinomas, 1 small cell carcinoma, and 1 large cell carcinoma), five metastases, and six benign lesions (2 chronic fibrotic inflammation, 3 active pneumonia and 1 schwannoma). Histopathological diagnoses were obtained after lung biopsy or surgical resection in all lung carcinomas and in four benign pulmonary lesions. The five pulmonary metastases with histologically confirmed primary tumors were initially detected by CT (n = 3) and PET/CT (n = 2) and confirmed by follow-up examination (after an average time of 4.6 months). Two pulmonary lesions were diagnosed as inflammatory consolidations because size was regressive on CT and x-ray during a 3-month follow-up examination. None of the 25 lesions had apparent cavitation and calcification on CT images. All lesions had a size larger than 12 mm. The mean size (\pm standard deviation) of the lesions was 47 ± 22 mm (range from 12 to 82 mm) for the malignant cases and 41 ± 42 mm (range from 16 to 125 mm) for the benign cases, with the long axis diameter of the pulmonary lesions determined on CT images.

All lesions with exception of one (schwannoma) were examined by integrated PET/CT (n = 24). DWI and PET/CT imaging were performed within a 2-week interval. For organizational reasons, in five patients MRI and PET/CT could not be performed until the first, respectively the second cycle of chemotherapy (n = 4 adenocarcinoma, n = 1 squamous cell carcinoma, n = 3 metastases).

MR Protocol

All examinations were performed on a clinical 3.0-T whole-body MRI system (Achieva 3.0T TX; Philips Healthcare,

Best, The Netherlands; gradient system: 80 mT/m maximum amplitude, 0.16 ms minimal rise time, 200 T/m/s maximum slew rate; actively shielded gradient coil, equipped with dual-source RF transmission technology) using a commercially available phased array surface receiver coil (SENSE-XL-TORSO). A single-shot spin-echo echo-planar imaging DWIBS sequence with two b-values (b = 0, 1000 s/mm²) was applied during free breathing (Table 1) after a high-order volume B0 shim was performed. Isotropic diffusion-weighted images were calculated. In 6 patients (8 lesions), additionally a DWIBS sequence with three b-values (b = 0, 50, 1000 s/mm²) was applied. After image acquisition, full MIP reconstruction for the isotropic b = 1000 s/mm² images and apparent diffusion coefficient (ADC) map calculation were carried out on the console. Hereby ADC(0,1000) maps were calculated from b = 0 and 1000 s/mm² and ADC(50,1000) maps from b = 50 and 1000 s/mm².

Except DWI, conventional coronal T1-weighted spin-echo (repetition time TR in ms/echo time TE in ms/number of excitations: 720/20/1) and coronal and axial T2-weighted fast spin-echo (6700/130/1) images were acquired (section thickness: 6 mm, intersection gap: 1 mm, field of view: 32 cm, matrix: 256 x 192).

Table 1: Sequence parameters of the used DWIBS protocol using dual-source (TX) RF excitation. Values are given for the two b-value variant. If values deviate for the three b-value variant they are given in square brackets.

Name	Value
Field of view (RLxAPxFH) / orientation	400 x 339 x 280 mm / transversal
Number of slices / thickness / gap	80 / 3.5 mm / 0 mm
Matrix / resolution	132 x 112 / 3.0 x 3.0 mm
TE	41 ms
TR	\approx 19000 ms
EPI- / half-Fourier- / SENSE-factor	47 / 0.638 / 2.5
Diffusion gradients	3 orthogonal directions
b-values (number of averages)	0 s/mm ² (NSA = 2) and 1000 s/mm ² (NSA = 3) [50 s/mm ² (NSA=2)]
Fat suppression methods	STIR + SSGR
STIR: TI	260 ms
Acquire during delay	Yes
WFS / BW / BW in EPI freq. direction	14.8 Pixel / 29.3 Hz / 3644 Hz
Acquisition time	6:39 min [8:16 min]

Abbreviations: RL - right-left direction, AP - anterior-posterior direction, FH - feet-head direction, EPI - echo-planar imaging, TE - echo time, TR - repetition time, SENSE - parallel imaging with sensitivity encoding, STIR - short TI inversion recovery, TI - inversion time, WFS - water fat shift, BW - band width, SSGR - slice-selective gradient reversal.

PET/CT

PET/CT was performed using a Somatom Emotion Duo scanner (Siemens, Erlangen, Germany). CT slices and PET emission data were acquired from the skull to the mid-thigh. All patients fasted for at least 8 hours prior to FDG injection. Serum

glucose levels did not exceed 160 mg/dl in any patient. Image acquisition started 60 min after intravenous injection of 370 to 550MBq of FDG. CT scan was performed after intravenous injection of contrast medium (Ultravist 300®, Bayer Healthcare, Leverkusen, Germany). To achieve a parenchymal contrast, a bolus of 80 ml was injected with a flow of 2 ml/s and the scan was started with a delay of 60 s. CT was acquired with the following parameters: 130 kV, 160 mAs, slice thickness 5 mm, increment 4.25 mm, pitch 1.5, rotation time 0.5 s. The PET acquisition was started immediately after CT imaging. Acquisition time was 4.5 min per bed position (5 - 8 bed positions per patient). Each position had 35 scanning planes with a 14.6 cm longitudinal field of view and a 1-slice overlap between scanning positions. CT and PET images were matched and fused into axial images of 4.25 mm thickness.

Qualitative Analysis of DWIBS and PET/CT Images

The sensitivity and specificity of detecting malignant lesions was investigated for DWIBS and FDG PET images. Hereby, the patient with the schwannoma was not included, because no PET/CT was available. Histological results served as gold standard. The qualitative analysis of FDG PET images was performed by one board-certified specialist for nuclear medicine together with a board-certified radiologist. The reader was unaware of the patients' clinical data. All suspected pulmonary and mediastinal lesions were identified on the PET/CT images and then visually judged on the FDG PET images with respect to their FDG-uptake. DWIBS images were evaluated qualitatively by 2 board-certified radiologists with 13 and 6 years of clinical MRI experience and one physicist with more than 16 years of experience in DWI. The readers were unaware of the patients' clinical data. The suspected lesions on CT images were identified on the diffusion-weighted $b = 1000$ s/mm² images with respect to hyperintensity.

Quantitative Analysis of DWIBS Images

All hyperintense lesions on $b = 1000$ s/mm² images were quantitatively analysed by ADC and lesion-to-spinal cord ratio (LSR) determination by the same readers as before. An elliptic or a freehand-drawn region of interest (ROI), as large as possible, was carefully placed on the DWI $b = 1000$ s/mm² image by adapting the ROI to the most hyperintense structures (lowest ADC values) in order to better characterize malignancy in case of heterogeneity^[21] or obstructive consolidation^[11,22]. We excluded necrotic areas, areas close to the lesion rim to avoid partial-volume effects, and areas with obvious motion or susceptibility artefacts. After visually cross-checking for pixel misalignments between images with different b values, the ROI was copied into the ADC parameter map. For the repeated measurements, the same shape and size of the ROIs were used, but ROIs were adapted to the actual lesion position. For LRS analysis, the mean signal intensity within the chosen ROI and within the spinal cord was analyzed on the same $b = 1000$ s/mm² image. The ADC(0,1000) and LSR values of the two b -value data sets were analyzed with respect to differences between malignant and benign lesions and between histological subgroups. These analyses were performed twice, once with the whole data set and once with reduced data set where treated lesions were excluded in order to avoid ADC confounding/blurring induced by therapy.

From repeated data, an intra-subject coefficient of vari-

ation (CV) of ADC(0,1000) and LSR values was determined, whereby CV was calculated as the standard deviation of the parameters belonging to the two measurements divided by the mean of the measured values.

At last, the three b -value data sets were analyzed with respect to differences between the ADC(0,1000) and ADC(50, 1000) values. This analysis was performed twice, once with the whole data set and once with reduced data set where treated lesions were excluded.

Statistical Analysis

The results of visual judgment were analyzed using a binary classification test. Statistical significance ($P < 0.05$) of differences between two groups was tested using the Mann-Whitney U test in case of independent samples and Wilcoxon signed-rank test in case of paired samples. For analysis of multiple independent subgroups the Kruskal-Wallis test was performed. Statistics were performed in SPSS (version 21.0, IBM, Armonk, NY, USA).

Results

Qualitative Analysis of DWIBS and PET/CT Images

All malignant lesions ($n = 19$) appeared hyperintense on $b = 1000$ s/mm² images and also on FDG PET images. Among the benign lesions, 40% (2 of 5 lesions) appeared hyperintense on DWIBS (1 chronic fibrotic lesion, 1 active pneumonia) and 60% (3 of 5 lesions) on PET (2 chronic fibrotic lesions, 1 active pneumonia) (see Table 2). An example is given in Figure 1.

Table 2: Results of visual judgment for detecting malignant lesions with diffusion-weighted imaging (DWI) and positron emission tomography imaging (FDG PET). Histological results were reference standard. The numbers of positive and negative results are given.

Subgroup	DWI		FDG PET images	
	Positive	Negative	Positive	Negative
Malignant ($n = 19$)	19	0	19	0
- Adenocarcinoma ($n = 9$)	9	0	9	0
- Squamous cell carcinoma ($n = 3$)	3	0	3	0
- Small cell carcinoma ($n = 1$)	1	0	1	0
- Large cell carcinoma ($n = 1$)	1	0	1	0
- Pulmonal metastases ($n = 5$)	5	0	5	0
Benign ($n = 5$, schwannoma excluded)	2	3	3	2
- Active pneumonia ($n = 3$)	1	2	1	2
- Chronic fibrotic inflammation ($n = 2$)	1	1	2	0
[- Schwannoma ($n = 1$)]	[1]	[0]	-	-

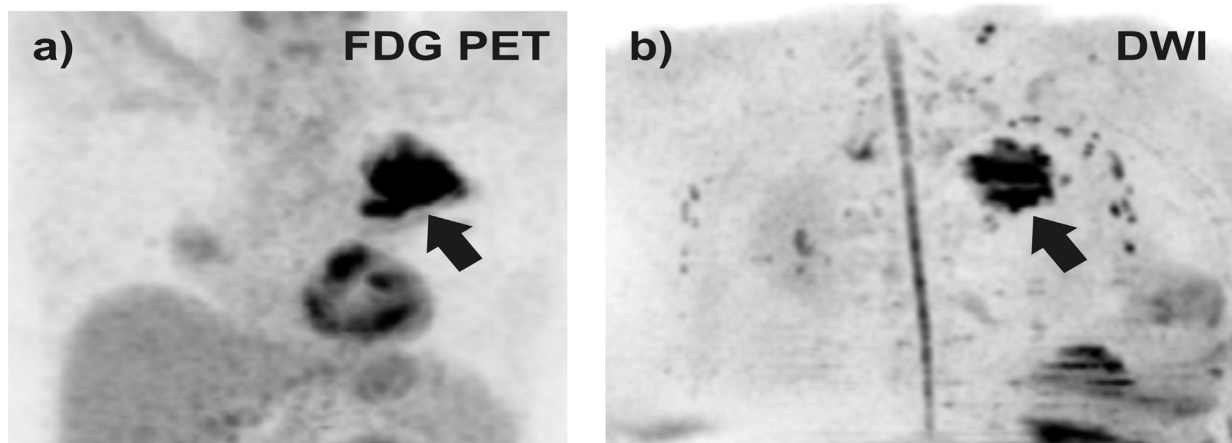


Figure 1: DWIBS and FDG PET images performed in a 77 year old patient with adenocarcinoma of histological grade 2. The pulmonary lesion (see arrow) was visible on a) FDG PET and b) DWIBS image. Both images were reconstructed by full-volume MIP reconstruction for the axial source images followed by grey scale inversion.

Quantitative Analysis of DWIBS Images

The ROI sizes (mean \pm standard deviation) of analyzed lesions were $92 \pm 124 \text{ mm}^2$ (range: 10 - 496 mm^2) and of spinal cord $17 \pm 10 \text{ mm}^2$ (range: 8 - 39 mm^2). The results of $\text{ADC}(0,1000)$ and LSR value analysis are summarized in Table 3. An example is given in Figure 2. For the malignant lesion group compared to the benign lesion group, lower $\text{ADC}(0,1000)$ values and higher LSR values were found (1074 ± 204 vs 1171 ± 260 and 2.34 ± 0.96 vs 1.79 ± 0.30 , respectively, when treated lesions are excluded), however, the differences were not statistically significant, neither for the whole data set nor for the reduced data set of untreated lesions. Despite the low case numbers, a subgroup analysis was attempted between histopathological subgroups of malignant lesion, but unfortunately no significant differences were found. By tendency, smaller $\text{ADC}(0,1000)$ values were found for squamous cell carcinoma compared to adenocarcinomas (855 ± 26 vs 1237 ± 169 , $P = 0.095$). For LSR values neither a significant difference nor a general trend was observed.

Table 3: Apparent diffusion coefficient $\text{ADC}(0,1000)$ and lesion-to-spinal cord ratio (LSR) for the different histopathology types of lung carcinomas, metastases, and benign lesions (only those with hyper intensity on $b = 1000 \text{ s/mm}^2$ image). Mean values \pm inter individual standard deviations are given for each subgroup. For subgroups including treated lesions, the data without those lesions were also listed (after forward slash). Results of statistical comparisons for groups with $n \geq 3$ are given. For $P > 0.100$ the abbreviation ns for not significant was used, for $0.5 \leq P \leq 0.100$ values were given in round brackets indicating that the values are different by tendency.

Subgroup	$\text{ADC}(0,1000)$ [$10^{-6} \text{ mm}^2/\text{s}$]	LSR
Malignant (n = 19 / n = 11)	1033 ± 220 / 1074 ± 204	2.14 ± 0.87 / 2.34 ± 0.96
- Adenocarcinoma (n = 9 / n = 5)	1089 ± 256 / 1237 ± 169	2.04 ± 0.61 / 2.11 ± 0.73
- Squamous cell carcinoma (n = 3 / n = 2)	857 ± 19 / 855 ± 26	2.79 ± 0.74 / 3.13 ± 0.65
- Small cell carcinoma (n = 1)	1116	1.57
- Large cell carcinoma (n = 1)	863	0.91
- Pulmonal metastases (n = 5 / n = 2)	1057 ± 214 / 971 ± 77	2.29 ± 1.26 / 3.21 ± 0.99
Benign (n = 3)	1171 ± 260	1.79 ± 0.30
- Active pneumonia (n = 1)	1471	1.83
- Chronic fibrotic inflammation (n = 1)	1025	1.47
- Schwannoma (n = 1)	1018	2.06
Results of group comparisons:		
P(malignant, benign)	ns / ns	ns / ns
P(adenocarcinoma, squamous cell carcinoma)	ns / (0.095)	ns / ns
P(adenocarcinoma, metastases)	ns / ns	ns / ns
P(adenocarcinoma, benign)	ns / ns	ns / ns
P(squamous cell carcinoma, metastases)	ns / ns	ns / ns
P(squamous cell carcinoma, benign)	ns / ns	ns / ns
P(metastases, benign)	ns / ns	ns / ns

The comparison between data of the first and repeated measurement (whole data set) did not reveal any significant differences, neither for $\text{ADC}(0,1000)$ nor for LSR values. The mean intra-individual coefficient of variation (CV) of $\text{ADC}(0,1000)$ values was 2.9% and of LSR values 23.9%, which is more than a factor of 8 higher. This difference was statistically significant ($P = 0.012$).

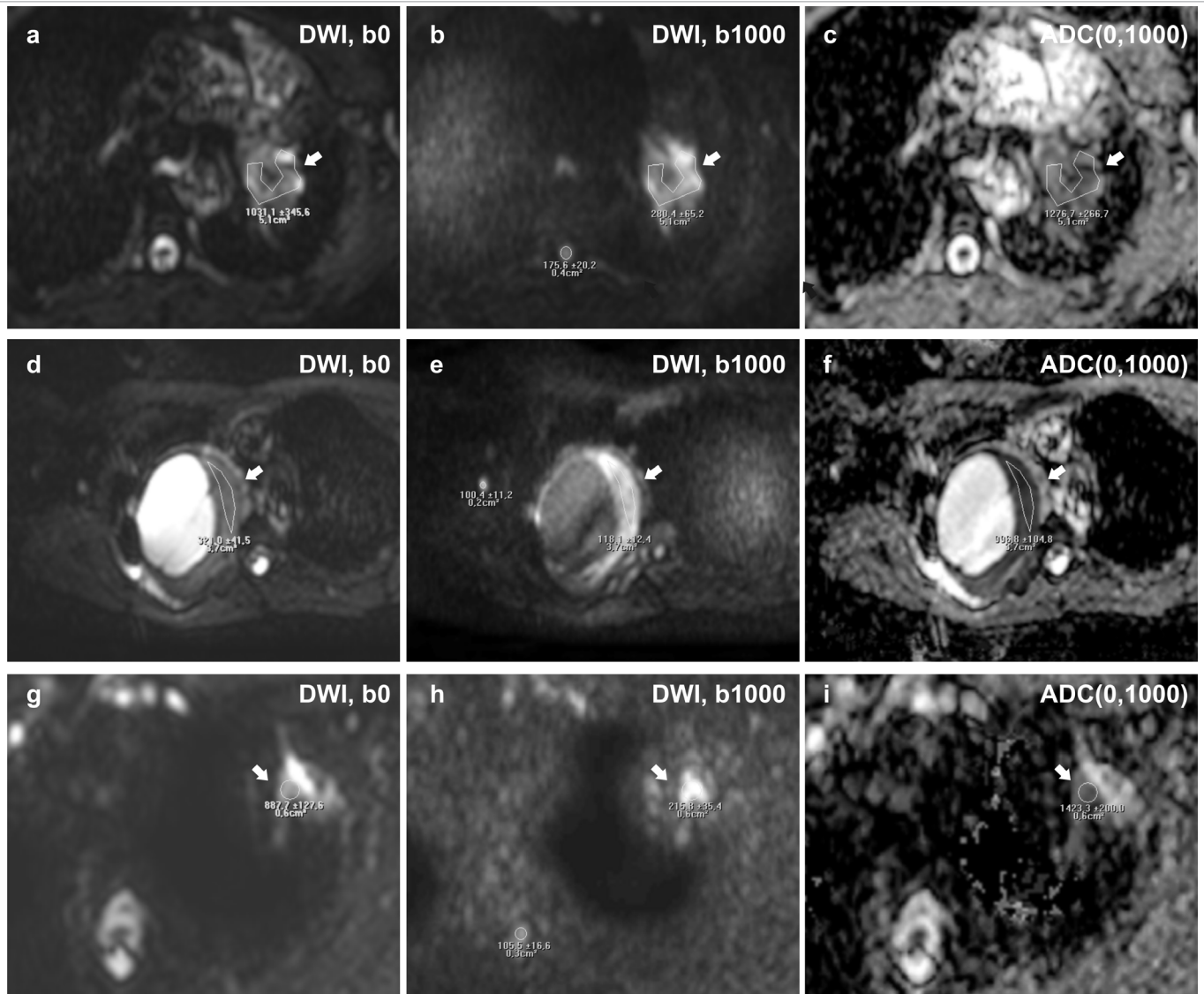


Figure 2: Axial Diffusion-Weighted Imaging (DWI) performed on a 56-year old patient with an adenocarcinoma of histological grade 3 (see arrow) (a-c), a 49-year old patient with a schwannoma (see arrow) (d-e), and a 67-year old patient with active pneumonia (see arrow). The ADC(0,1000) given in mm²/s of the adenocarcinoma is higher than that in the solid part of the schwannoma (997 ± 105) and lower than of the pneumonia (1423 ± 200). The lesion-to-spinal cord ratio (LSR) of the adenocarcinoma (1.60) is higher than in the schwannoma (1.18) and lower than in the pneumonia (2.05). The coefficients of variations of the ADC(0,1000) values were lower (1.7% for the adenocarcinoma and 10.4% for the schwannoma) than for the LSR (12.4% for the adenocarcinoma, 33.3% for the schwannoma). For pneumonia no 3-b-value sequence was acquired. Differences between ADC(0,1000) and ADC(50,1000) were 10.1% in the adenocarcinoma and 8.0% in the schwannoma.

Table 4: Apparent diffusion coefficients ADC(0,1000) and ADC(50,1000) as well as relative differences between them (rel. diff.) obtained from the three b-value sequence for the different histopathology types of lung carcinomas, metastases, and benign lesions (only those with hyper intensity on b = 1000 s/mm² image). Mean values ± inter individual standard deviations are given for each subgroup. For subgroups including treated lesions, the data without those lesions were also listed (after forward slash).

Subgroup	ADC(0,1000) [10 ⁻⁶ mm ² /s]	ADC(50,1000) [10 ⁻⁶ mm ² /s]	Rel. diff. [%]
Malignant (n = 7 / n = 5)	1101 ± 262 / 1132 ± 241	1010 ± 244 / 1033 ± 240	9.4 / 10.4
- Adenocarcinoma (n = 3 / n = 2)	1157 ± 372 / 1365 ± 125	1082 ± 341 / 1268 ± 154	6.6 / 7.8
- Squamous cell carcinoma (n = 1)	836	865	-3.4
- Small cell carcinoma (n = 1)	1103	983	12.2
- Large cell carcinoma (n = 0)			
- Pulmonal metastases (n = 2 / n = 1)	1151 ± 224 / 992	988 ± 295 / 780	18.3 / 27.3
Benign (n = 1)	1180	1093	8.0
- Active pneumonia (n = 0)			
- Chronic fibrotic inflammation (n = 0)			
- Schwannoma (n = 1)	1180	1093	8.0
Total (n = 8 / n = 6)	1111 ± 244 / 1140 ± 217	1020 ± 228 / 1043 ± 216	9.2 / 10.0

The ADC(0,1000) and ADC(50, 1000) values obtained from the three b-value sequence are summarized in Table 4. Including all data, the ADC(50, 1000) values were significantly lower than the ADC(0,1000) values (1020 ± 228 compared to 1111 ± 244 , $P = 0.016$). This was also found by tendency for the reduced data set of untreated lesions (1043 ± 216 compared to 1140 ± 217 , $P = 0.063$). The mean difference between ADC(0,1000) and ADC(50, 1000) values was largest for the metastases (27.3%), medium for adenocarcinoma and benign lesions (7.8% and 8.0%, respectively), and lowest for squamous cell carcinoma ($< 0.1\%$).

Discussion

The aim of this work was to gain more experience with DWIBS at 3.0 T for pulmonary lesion detection and characterization. The lesion detectability of DWIBS was comparable with FDG PET. Concerning lesion characterization, quantitative analysis of apparent diffusion coefficient ADC(0,1000) was superior to lesion-to-spinal cord ratio LSR with respect of repeatability. The use of 3 instead of 2 b-values enabled additional information about perfusion influences. The acquisition technique was “state of the art” with dual-source RF transmission technology, parallel imaging with sensitivity encoding (SENSE), and advanced fat suppression methods. The sequence was optimized for the equipment previously^[13,14].

The rough comparison between DWIBS and FDG PET imaging revealed very high sensitivity of detecting malignant lesions (100%) for both modalities. The specificity was worse with 40% false positive results in case of DWIBS and 60% for FDG PET. The results of this study are in general agreement with previous studies. However, results may depend on group compositions. In our study, no bronchioloalveolar cancers or mucinous adenocarcinomas were included. In other studies, false negative results in FDG PET studies occurred in bronchioloalveolar cancers, whereas DWI failed in case of mucinous adenocarcinomas^[7] or if lesions were affected by cardiac motion^[23]. Moreover, in our study, the benign lesion group contained active pneumonia and chronic fibrotic inflammation, which were partly detected as false-positive. For the active pneumonia the number of false positive results was the same for both modalities, whereas for chronic fibrotic inflammation more false positive results were detected by FDG PET. In other studies, a similar or higher number of active inflammatory lesions and chronic inflammation were detected as false-positive by FDG PET compared to DWI^[6,7,16,20,21,24]. The sensitivity reported in other studies was found to be similar or superior for conventional DWI compared to FDG PET^[6,7,16,21,24], with exception of one study reporting inferior sensitivity^[23]. The specificity was found to be comparable between FDG PET and conventional DWI at 1.5 and 3.0 T and DWIBS at 1.5 T^[6,7,16,24], with exception of one study reporting superior specificity for DWI^[21]. As both diagnostic modalities have their specific strengths and weaknesses^[7,16], the combined use of DWI and FDG PET using PET MRI scanners, may provide beneficial with respect to diagnostic accuracy^[20,21].

For lesion characterization with DWI, different methods have been used: e.g. visual inspection of signal intensity in comparison to muscle or spinal cord, semiquantitative analysis of lesion-to-spinal cord signal intensity ratio (LSR), or quantitative determination of the apparent diffusion coefficient (ADC)^[3,4,7,21,25-27]. At 1.5 T, it remained unclear which analysis method

should be preferred^[4,26,27]. For 3.0 T up to now no comparative study exists. In our study, malignant lesions had by tendency lower ADC(0,1000) values and higher LSR values than lesions in the benign group, a finding that had been reported before at 1.5 T^[4,16,25-28]. The larger diffusion restriction in malignant lesions is usually attributed to higher cellularity^[29], as there is an inverse correlation between ADC and tumor cellularity^[15]. ADC and LSR values, however, may also be affected by the amount of intracellular macromolecular proteins, cell proliferation, extracellular space relative to normal tissue, and by perfusion^[15]. In addition, diffusion restriction can be affected by necrosis, abscesses, and thrombi^[25]. Thus, the broad overlapping of ADC values in some studies and the varying differentiability between different studies may be caused by differences in group composition. Subgroup analysis in our work provides only little information due to the low case numbers of some subgroups. However, a lower ADC(0,1000) value for squamous cell carcinoma compared to adenocarcinoma was found by tendency, no such tendency was found for LSR. This is in accordance with previous work, in which significantly higher cellularity of squamous cell carcinoma compared to adenocarcinomas was found^[15,30]. In case of ADC determination, values were calculated from at least two b-values and the error of signal intensity due to motion and susceptibility artefacts at each b-values is propagated^[26]. Moreover, some benign lesions showed low ADC values similar to malignant lesions^[26]. In case of LSR analysis, values reflect a combined effect of diffusion restriction and T2 (and T1) elongation, which intensifies the signal intensity of malignant lesions, but may also occur in some benign situations such as cryptogenic organizing pneumonia^[26]. A problem with signal intensity ratios may exist if the standard of reference is inaccurate due to partial volume effects or pathologically changed as in case of inflamed or fatty muscles. To reduce the influence of susceptibility artefacts and partial volume effects, in the presented 3.0 T study small ROIs were used, not including the margin of the lesion or spinal cord. Even if it remains unclear which method is superior for lesion differentiation our results suggest that ADC(0,1000) values provide a significantly better repeatability than LSR values. Thus, for lesion characterization (and therapy monitoring) the ADC(0,1000) determination seems to be superior to the LSR quantification.

The ADC is generally affected by both molecular diffusion and microcirculation effects^[31] as shown in an initial study for lung carcinomas^[11]. Therefore, reported values vary between different studies, depending on the b-values and acquisition methods used. The use of more than two b-values in DWI allows for separation of tissue diffusivity and blood perfusion effects as proposed by the Intra Voxel Incoherent Motion (IVIM) model^[31]. In first studies on pulmonary lesions, IVIM has been applied for differentiation between cancer and obstructive consolidation^[11], and between malignant and benign masses or consolidations^[32,33]. Lower perfusion fractions were found for lung cancer compared to obstructive consolidation^[11] and inflammatory lesions^[32], but no differences in perfusion effects were found between malignant and benign masses^[33]. In the presented 3.0 T study, in addition to b-values of 0 and 1000 s/mm², a low b-value of 50s/mm² was included in the sequence for a rough assessment of perfusion effects. From the used three b-values it is possible to obtain perfusion sensitive biomarkers as ADC(0, 50)^[34], estimation of perfusion fraction^[35-40] or simply the ADC

difference between the conventionally used ADC(0,1000) and the ADC(50, 1000), which is less affected by perfusion effects, as in the present study. With this simplified IVIM approach, a further separation into perfusion fraction and pseudodiffusion coefficient as obtained for full IVIM approaches is not possible. Perfusion influences were found to be especially large for metastases, followed by adenocarcinoma and benign lesions, whereas they seemed to be low for squamous cell carcinoma. Thus, IVIM analyses seem to provide important data for characterization of pulmonary lesions, which should be investigated further in future studies.

Limitations of the study were the limited number of patients, and that not all patients were examined before treatment. Repeated measurements could not be performed in all patients, but sufficient statistical power was reached for the analysis of repeatability between LSR and ADC(0,1000). The results were meaningful and allowed a suggestion for analysis strategy in further studies.

In conclusion, this study indicates the potential of DWIBS at 3.0 T for detecting and characterizing pulmonary lesions. Lesion detection using DWIBS was as good as with FDG PET. For lesion characterization, ADC analysis was superior to signal intensity ratio determination with respect to repeatability. Moreover, an analysis of perfusion influences provides additional information.

Acknowledgement: There are no conflicts of interest.

References

- [1] Zhang, C.Y., Yu, H.L., Li, X., et al. Diagnostic value of computed tomography scanning in differentiating malignant from benign solitary pulmonary nodules: a meta-analysis. (2014) *Tumour Biol* 35(9): 8551–8558.
[Pubmed](#) | [Crossref](#) | [Others](#)
- [2] Cronin, P., Dwamena, B.A., Kelly, A.M., et al. Solitary pulmonary nodules: meta-analytic comparison of cross-sectional imaging modalities for diagnosis of malignancy. (2008) *Radiology* 246(3): 772–782.
[Pubmed](#) | [Crossref](#) | [Others](#)
- [3] Luna, A., Sanchez-Gonzalez, J., Caro, P. Diffusion-weighted imaging of the chest. (2011) *Magn Reson Imaging Clin N Am* 19(1): 69–94.
[Pubmed](#) | [Crossref](#) | [Others](#)
- [4] Liu, H., Liu, Y., Yu, T., et al. Usefulness of diffusion-weighted MR imaging in the evaluation of pulmonary lesions. (2010) *Eur Radiol* 20(4): 807–815.
[Pubmed](#) | [Crossref](#)
- [5] Chen, L., Zhang, J., Bao, J., et al. Meta-analysis of diffusion-weighted MRI in the differential diagnosis of lung lesions. (2013) *J Magn Reson Imaging* 37(6): 1351–1358.
[Pubmed](#) | [Crossref](#) | [Others](#)
- [6] Nomori, H., Cong, Y., Sugimura, H., et al. Comparing diffusion-weighted imaging and positron emission tomography for pulmonary nodules measuring from 1 to 3 cm in size. (2015) *Surg Today* 45(12): 1535–1541.
[Pubmed](#) | [Crossref](#) | [Others](#)
- [7] Usuda, K., Sagawa, M., Motono, N., et al. Diagnostic performance of diffusion weighted imaging of malignant and benign pulmonary nodules and masses: comparison with positron emission tomography. (2014) *Asian Pac J Cancer Prev* 15(11): 4629–4635.
[Pubmed](#) | [Crossref](#)
- [8] Usuda, K., Sagawa, M., Motono, N., et al. Recurrence and metastasis of lung cancer demonstrate decreased diffusion on diffusion-weighted magnetic resonance imaging. (2014) *Asian Pac J Cancer Prev* 15(16): 6843–6848.
[Pubmed](#) | [Crossref](#)
- [9] Coolen, J., Vansteenkiste, J., De, K.F., et al. Characterisation of solitary pulmonary lesions combining visual perfusion and quantitative diffusion MR imaging. (2014) *Eur Radiol* 24(2): 531–541.
[Pubmed](#) | [Crossref](#)
- [10] Koyama, H., Ohno, Y., Nishio, M., et al. Diffusion-weighted imaging vs STIR turbo SE imaging: capability for quantitative differentiation of small-cell lung cancer from non-small-cell lung cancer. (2014) *Br J Radiol* 87(1038): 20130307.
[Pubmed](#) | [Crossref](#)
- [11] Wang, L.L., Lin, J., Liu, K., et al. Intravoxel incoherent motion diffusion-weighted MR imaging in differentiation of lung cancer from obstructive lung consolidation: comparison and correlation with pharmacokinetic analysis from dynamic contrast-enhanced MR imaging. (2014) *Eur Radiol* 24(8): 1914–1922.
[Pubmed](#) | [Crossref](#) | [Others](#)
- [12] Takahara, T., Imai, Y., Yamashita, T., et al. Diffusion weighted whole body imaging with background body signal suppression (DWIBS): technical improvement using free breathing, STIR and high resolution 3D display. (2004) *Radiat Med* 22(4): 275–282.
[Pubmed](#) | [Others](#)
- [13] Mürtz, P., Kaschner, M., Traber, F., et al. Evaluation of dual-source parallel RF excitation for diffusion-weighted whole-body MR imaging with background body signal suppression at 3.0 T. (2012) *Eur J Radiol* 81(11): 3614–3623.
[Pubmed](#) | [Crossref](#) | [Others](#)
- [14] Mürtz, P., Kaschner, M., Traber, F., et al. Diffusion-weighted whole-body MRI with background body signal suppression: Technical improvements at 3.0 T. (2012) *J Magn Reson Imaging* 35(2): 456–461.
[Pubmed](#) | [Crossref](#) | [Others](#)

- [15] Chen, L., Zhang, J., Chen, Y., et al. Relationship between apparent diffusion coefficient and tumour cellularity in lung cancer. (2014) *PLoS One* 9(6): e99865.
[Pubmed](#) | [Crossref](#) | [Others](#)
- [16] Zhang, J., Cui, L.B., Tang, X., et al. DW MRI at 3.0 T versus FDG PET/CT for detection of malignant pulmonary tumors. (2014) *Int J Cancer* 134(3): 606–611.
[Pubmed](#) | [Crossref](#) | [Others](#)
- [17] Tanaka, R., Nakazato, Y., Horikoshi, H., et al. Diffusion-weighted imaging and positron emission tomography in various cytological subtypes of primary lung adenocarcinoma. (2013) *Clin Imaging* 37(5): 876–883.
[Pubmed](#) | [Crossref](#) | [Others](#)
- [18] Cui, L., Yin, J.-B., Hu, C.-H., et al. Inter- and intraobserver agreement of ADC measurements of lung cancer in free breathing, breath-hold and respiratory triggered diffusion-weighted MRI. (2016) *Clin Imaging* 40(5): 892–896.
[Pubmed](#) | [Crossref](#) | [Others](#)
- [19] Mesmann, C., Sigovan, M., Berner, L.-P., et al. Evaluation of image quality of DWIBS versus DWI sequences in thoracic MRI at 3 T. (2014) *Magn Reson Imaging* 32(10): 1237–1241.
[Pubmed](#) | [Crossref](#) | [Others](#)
- [20] Schmidt, H., Brendle, C., Schraml, C., et al. Correlation of simultaneously acquired diffusion-weighted imaging and 2-deoxy-[18F] fluoro-2-D-glucose positron emission tomography of pulmonary lesions in a dedicated whole-body magnetic resonance/positron emission tomography system. (2013) *Invest Radiol* 48(5): 247–255.
[Pubmed](#) | [Crossref](#) | [Others](#)
- [21] Mori, T., Nomori, H., Ikeda, K., et al. Diffusion-weighted magnetic resonance imaging for diagnosing malignant pulmonary nodules/masses: comparison with positron emission tomography. (2013) *J Thorac Oncol* 8(4): 358–364.
[Pubmed](#) | [Crossref](#) | [Others](#)
- [22] Baysal, T., Mutlu, D.Y., Yologlu, S. Diffusion-weighted magnetic resonance imaging in differentiation of postobstructive consolidation from central lung carcinoma. (2009) *Magn Reson Imaging* 27(10): 1447–1454.
[Pubmed](#) | [Crossref](#) | [Others](#)
- [23] Komori, T., Narabayashi, I., Matsumura, K., et al. 2-[Fluorine-18]-fluoro-2-deoxy-D-glucose positron emission tomography/computed tomography versus whole-body diffusion-weighted MRI for detection of malignant lesions: initial experience. (2007) *Ann Nucl Med* 21(4): 209–215.
[Pubmed](#) | [Crossref](#) | [Others](#)
- [24] Ohba, Y., Nomori, H., Mori, T., et al. Diffusion-weighted magnetic resonance for pulmonary nodules: 1.5 vs. 3 Tesla. (2011) *Asian Cardiovasc Thorac Ann* 19(2): 108–114.
[Pubmed](#) | [Crossref](#) | [Others](#)
- [25] Shen, G., Jia, Z., Deng, H. Apparent diffusion coefficient values of diffusion-weighted imaging for distinguishing focal pulmonary lesions and characterizing the subtype of lung cancer: a meta-analysis. (2016) *Eur Radiol* 26(2): 556–566.
[Pubmed](#) | [Crossref](#) | [Others](#)
 PMID:26003791
- [26] Uto, T., Takehara, Y., Nakamura, Y., et al. Higher sensitivity and specificity for diffusion-weighted imaging of malignant lung lesions without apparent diffusion coefficient quantification. (2009) *Radiol* 252(1): 247–254.
[Pubmed](#) | [Crossref](#)
- [27] Çakmak, V., Ufuk, F., Karabulut, N. Diffusion-weighted MRI of pulmonary lesions: Comparison of apparent diffusion coefficient and lesion-to-spinal cord signal intensity ratio in lesion characterization. (2016) *J Magn Reson Imaging* 45(3): 845–854.
[Pubmed](#) | [Crossref](#)
- [28] Satoh, S., Kitazume, Y., Ohdama, S., et al. Can malignant and benign pulmonary nodules be differentiated with diffusion-weighted MRI? *AJR Am J Roentgenol* 191(2): 464–470.
[Pubmed](#) | [Crossref](#) | [Others](#)
- [29] Chen, L., Liu, M., Bao, J., et al. The correlation between apparent diffusion coefficient and tumor cellularity in patients: a meta-analysis. (2013) *PLoS One* 8(11): e79008.
[Pubmed](#) | [Crossref](#) | [Others](#)
- [30] Razek, A.A., Fathy, A., Gawad, T.A. Correlation of apparent diffusion coefficient value with prognostic parameters of lung cancer. (2011) *J Comput Assist Tomogr* 35: 248–252.
[Crossref](#) | [Others](#)
- [31] Le Bihan, D., Breton, E., Lallemand, D., et al. Separation of diffusion and perfusion in intravoxel incoherent motion MR imaging. (1988) *Radiol* 168(2): 497–505.
[Pubmed](#) | [Crossref](#) | [Others](#)
- [32] Deng, Y., Li, X., Lei, Y., et al. Use of diffusion-weighted magnetic resonance imaging to distinguish between lung cancer and focal inflammatory lesions: a comparison of intravoxel incoherent motion derived parameters and apparent diffusion coefficient. (2015) *Acta Radiol* 57(11): 1310–1317.
[Pubmed](#) | [Crossref](#) | [Others](#)
- [33] Wang, X., Duan, J., Yuan, H. [Value of multiple b-value diffusion-weighted imaging for differentiation of benign and malignant pulmonary masses]. (2014) *Zhongguo Yi Xue Ke Xue Yuan Xue Bao* 36(5): 510–515.
[Pubmed](#) | [Others](#)
- [34] Kukuk, G.M., Mürtz, P., Träber, F., et al. Diffusion-weighted imaging with acquisition of three b-values for response evaluation of neuroendocrine liver metastases undergoing selective internal radiotherapy. (2014) *Eur Radiol* 24(2): 267–276.
[Pubmed](#) | [Crossref](#) | [Others](#)
- [35] Mürtz, P., Penner, A.-H., Pfeiffer, A.-K., et al. Intravoxel incoherent motion model-based analysis of diffusion-weighted magnetic resonance imaging with 3 b-values for response assessment in locoregional therapy of hepatocellular carcinoma. (2016) *Onco Targets and Therapy* 9: 6425–6433.
[Pubmed](#) | [Crossref](#) | [Others](#)
- [36] Pieper, C., Meyer, C., Sprinkart, A.M., et al. The value of intravoxel incoherent motion model-based diffusion-weighted imaging for outcome prediction in resin-based radioembolization of breast cancer liver metastases. (2016) *Onco Targets Ther* 9: 4089–4098.
[Pubmed](#) | [Crossref](#)
- [37] Pieper, C.C., Sprinkart, A.M., Meyer, C., et al. Evaluation of a Simplified Intravoxel Incoherent Motion (IVIM) Analysis of Diffusion-Weighted Imaging for Prediction of Tumor Size Changes and Imaging Response in Breast Cancer Liver Metastases Undergoing Radioembolization: A Retrospective Single Center Analysis. (2016) *Medicine (Baltimore)* 95(14): e3275.
[Pubmed](#) | [Crossref](#)
- [38] Pieper, C.C., Willinek, W.A., Meyer, C., et al. Intravoxel Incoherent Motion Diffusion-Weighted MR Imaging for Prediction of Early Arterial Blood Flow Stasis in Radioembolization of Breast Cancer Liver Metastases. (2016) *J Vasc Interv Radiol* 27(9):1320-8.
[Pubmed](#) | [Crossref](#) | [Others](#)
- [39] Decker, G., Mürtz, P., Gieseke, J., et al. Intensity-modulated radiotherapy of the prostate: dynamic ADC monitoring by DWI at 3.0 T. (2014) *Radiother Oncol* 113(1): 115–120.
[Pubmed](#) | [Crossref](#) | [Others](#)
- [40] Penner, A.-H., Sprinkart, A.M., Kukuk, G.M., et al. Intravoxel incoherent motion model-based liver lesion characterisation from three b-value diffusion-weighted MRI. (2013) *Eur Radiol* 23(10): 2773–2783.
[Pubmed](#) | [Crossref](#) | [Others](#)